MICROSTRUCTURE STUDY ON THE $La_{0.7}Sr_{0.3}MnO_3$ AND RARE-EARTH OXIDE VERTICALLY ALIGNED NANOCOMPOSITE THIN FILMS

A Senior Scholars Thesis

by

HARSHAD HAZARIWALA

Submitted to the Office of Undergraduate Research
Texas A&M University
in partial fulfillment of the requirements for the designation as

UNDERGRADUATE RESEARCH SCHOLAR

April 2011

Major: Electrical Engineering

MICROSTRUCTURE STUDY ON THE $La_{0.7}Sr_{0.3}MnO_3$ AND RARE-EARTH OXIDE VERTICALLY ALIGNED NANOCOMPOSITE THIN FILMS

A Senior Scholars Thesis

by

HARSHAD HAZARIWALA

Submitted to the Office of Undergraduate Research
Texas A&M University
in partial fulfillment of the requirements for the designation as

UNDERGRADUATE RESEARCH SCHOLAR

Approved by:

Research Advisor: Haiyan Wang
Director for Undergraduate Research: Sumana Datta

April 2011

Major: Electrical Engineering

ABSTRACT

Microstructure Study on the $La_{0.7}Sr_{0.3}MnO_3$ and Rare-earth Oxide
Vertically Aligned Nanocomposite Thin Films.
(April 2011)

Harshad Hazariwala
Department of Electrical and Computer Engineering
Texas A&M University

Research Advisor: Dr. Haiyan Wang
Department of Electrical and Electrical Engineering

Two-phase $(La_{0.7}Sr_{0.3}MnO_3)_{0.5}$:$(CeO_2)_{0.5}$ (LSMO:CeO_2) heteroepitaxial nanocomposite films were grown on $SrTiO_3$ (STO) (001) by pulsed laser deposition. XRD and TEM results show that LSMO:CeO_2 films epitaxially grow on STO as self-assembled vertically aligned nanocomposites (VAN). Magnetic and magnetotransport measurements demonstrate that the LSMO phases in the VAN structure behave differently from its epitaxial single phase counterpart. The greatly enhanced coercivity (H_C) and low field magnetoresistance (LFMR) in VAN system is attributed to the strong interaction between the pervoskite the secondary phase. Our results suggest that growth of functional oxide in another oxide matrix with vertical heteroepitaxial form is a promising approach to achieve new functionality which may not be obtained in the single epitaxial phase.

ACKNOWLEDGMENTS

I would like to thank the members of Wang's Thin Film Group for providing me with the opportunity and guidance to complete this research. Special thanks are owed to Professor Haiyan Wang and Ph.D candidates Aiping Chen and Zhenxing Bi.

This work was supported by the U.S. National Science Foundation (Ceramic Program, NSF-0709831 and NSF-1007969).

TABLE OF CONTENTS

LIST OF FIGURES

CHAPTER I

INTRODUCTION

Recently, there has been a growing interest in the coupling effects of different functions by combining the materials with suitable functions via multilayering or by forming vertical aligned nanocomposites hetero-epitaxially [1,2]. Unique properties that are not present in the single phase materials could be enabled in the vertical heteroepitaxial nanocomposite films due to the strong interfacial couplings at the phase boundaries. The epitaxial VAN films provide a larger vertical interfacial area where magnetoelectric coupling in $BaTiO_3$:$CoFe_2O_4$ and $BiFeO_3$:$NiFe_2O_4$, [3,4] and strain tuning in $BiFeO_3$:Sm_2O_3 and $La_{0.7}Sr_{0.3}MnO_3$:ZnO have been achieved. [5]

In this work, epitaxial $La_{0.7}Sr_{0.3}MnO_3$ and rare-earth oxide nanocomposites have been deposited on $SrTiO_3$ (001) single crystal substrates. The optimization of the deposition parameters including the oxygen pressure and temperature has been done to achieve better film quality for both phases and to achieve sharp columnar phase interfaces. At the beginning of the project, we processed ceramic composite targets by following the standard solid state reaction and analyze the target crystalline properties in order to

---

This thesis follows the style of Applied Physics Letters.

achieve deserved phases in the targets. After the thin films sample deposition, the microstructure and crystalling characterization of nanocomposite thin films have been done by the following methods, including X-ray diffraction (POWDER-SA, XRD), transmission electron microscopy (JEOL 2010, TEM). The cross-sectional TEM images can help identify the film microstructure and the electron diffraction pattern will help analyze different phase crystallinity and their epitaxial growth on the STO substrate. Here, CeO_2 was selected as the secondary phase for several reasons: (1) the good lattice matching of CeO_2 with STO and LSMO, as shown in Fig. 1(a) and 1(b). (2) the nonmagnetic insulating CeO_2 usually serving as an insulating layer in multilayer electronic devices. (3) the similar thermal expansion coefficient of CeO_2 (9.5×10^{-6}/K) with STO (10.4×10^{-6}/K) and LSMO (11.5×10^{-6}/K). (4) the refractory character and low reactivity minimizing the interdiffusion during the growth. Those characters make CeO_2 become a very promising candidate for realizing VAN with LSMO and achieving functionality. In this work, we investigated the microstructure, magnetic and low field magnetotransport in vertical heteroepitaxial $(La_{0.7}Sr_{0.3}MnO_3)_{0.5}$:$(CeO_2)_{0.5}$ nanocomposite thin films.

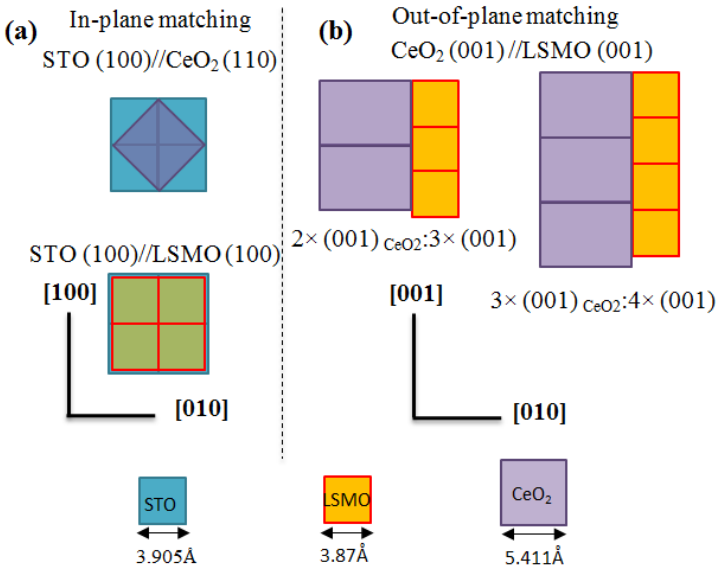

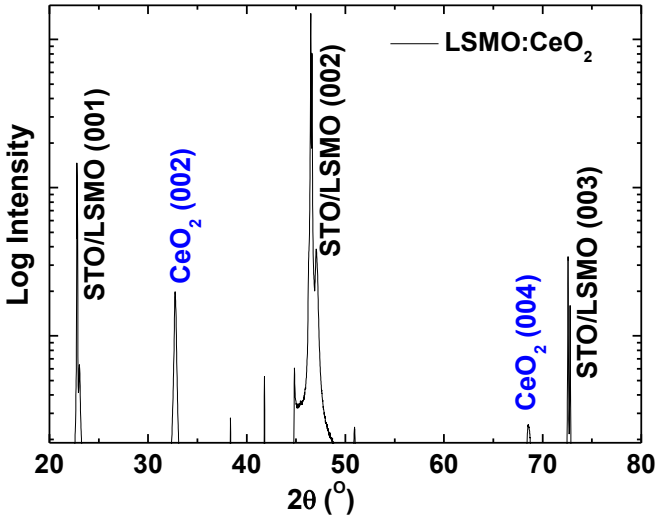

FIG. 1. 1(a) and (b) illustration of in-plane and out-of-plane lattice matching of among LSMO,CeO_2 and STO. (c) XRD result for the VAN films grown on STO (001) substrates (c) XRD result for the VAN films grown on STO (001) substrates.

CHAPTER II

METHODS

Ceramic composite targets were prepares using the standard solid state reaction. We mixed La_2O_3, $SrCO_3$ and MnO_2 powders according to proper Moore ratios. This is followed by grounding, pellet pressing and high temperature sintering in a tube furnace at 1450 ^{0}C with 150sccm oxygen flow for 12 hours. After forming pure LSMO phase, we mixed the pure LSMO powder with CeO_2 with a 1:1 Moore ratio to obtain a high density composite LSMO: CeO_2 composite target.

Pulsed laser deposition (PLD) was employed to grow LSMO:CeO_2 nanocomposite thin films on (001) oriented STO substrates with different repetition frequency (KrF laser, 248 nm). The laser beam was focused onto the target with an incidence angle of 45°, obtaining an energy density ~2.5 J/cm^2. An optimized substrate temperature of 750 °C and oxygen pressure of 200 mTorr were used during the deposition. After deposition, the films were cooled down to room temperature in an oxygen pressure of 200 Torr to assure proper film stoichiometry. The crystal structure, growth orientation and microstructure of the nanocomposite films were studied by X-ray diffraction (XRD) and transmission electron microscopy (TEM) (JEOL JEM-2010 and FEI Tecnai G2 F20 operation at 200 kV). The magnetic and magnetotransport properties of the nanocomposite thin films were systematically investigated on a commercial Physical Properties Measurement System (Quantum Design PPMS 6000). During the magnetic and transport

measurements, the magnetic field was applied perpendicular to the film plane and the current were performed in-plane.

CHAPTER III

RESULTS

Fig. 1(c) shows the XRD θ~2θ scan of a typical LSMO:CeO_2 nanocomposite film. It can be seen that only (00*l*) peaks were observed for both LSMO and CeO_2 phases, conforming that both phases have grown highly textured on STO (001) substrates. TEM was conducted to examine the microstructure of self-assembled VAN films deposited under different deposition frequencies. Figs. 2(a) and 2(b) show the cross-sectional TEM images for the LSMO:CeO_2 nanocomposite films on STO (001) deposited at 1 Hz and 10 Hz, respectively. It can be seen that the sub-10 nm domains are vertically aligned on substrates. Interestingly, the domain size is greatly reduced with increased deposition frequency with ~6 nm in 1 Hz and ~3 nm in 10 Hz. It may related to the reduced diffusion length of the adatoms as deposition frequency increases. The selected area electron diffraction (SAED) patterns, shown in Figs. 2(c) and 2(d), belong to 1 Hz and 10 Hz nanocomposite films, respectively. The distinct diffraction dots indicate high quality of the films. The diffraction dots of LSMO are connected by square and those of CeO_2 are labeled with diamond. The orientation relations between the 1 Hz LSMO:CeO_2 nanocomposite films and the substrates are determined to be LSMO (002) // CeO_2 (002) // STO (002), and LSMO [200] // CeO_2 [220] // STO [200]. It is quite interesting to note that there are two diamonds, perpendicular to each other, in 10 Hz sample diffraction pattern, indicating the CeO_2 phase exhibit double-epitaxial orientations in the 10 Hz nanocomposite film. The low mobility of adatoms and high epitaxial strain are the driving force for the formation of double-epitaxial Sr(Ti, Fe)O_3 films on CeO_2/YSZ

buffered Si substrates and double-epitaxial $LaFeO_3$ films on STO substrates. [6] Thus, short adatoms diffusion length in 10 Hz VAN films may favor the double-epitaxial growth of CeO_2 phase. A high resolution TEM image of 10 Hz LSMO:CeO_2 nanocomposite films in Fig. 2(e) shows an excellent epitaxial growth of LSMO and CeO_2 phases on STO substrate and those two phases are alternating with each other, indicating the self-assembly vertically aligned nanostructures. Large lattice mismatch between CeO_2 and LSMO (33.2 %) favor the domain matching along out-of-plane interface (2(3) planes of CeO_2 matching with 3(4) planes of LSMO) with relaxed strain of 7.0 % (4.8 %) [Fig. 1(b)].

Magnetic and magnetotransport properties of the films were shown in Fig. 3. H_C of pure epitaxial (PE) LSMO and 10 Hz VAN films are summarized in Fig. 3(a) and the H_C of both films decrease with increasing temperature as expected. It is worth noting that the H_C of the 10 Hz LSMO:CeO_2 VAN films are quite large (~820 Oe at 20 K) compared to both the PE LSMO deposited in this study and previous reports with the value of ~200 Oe (5 K). [7] The enhanced H_C of LSMO phase in VAN structure should be correlated with increased pinning effects from the phase boundaries. [8] It is not surprising that H_C tends to increase as the deposition repetition increases [inset of Fig. 3(a)]. It is because that the domain size is smaller at high deposition frequencies, resulting in more phase boundaries and higher pinning effect in the VAN films.

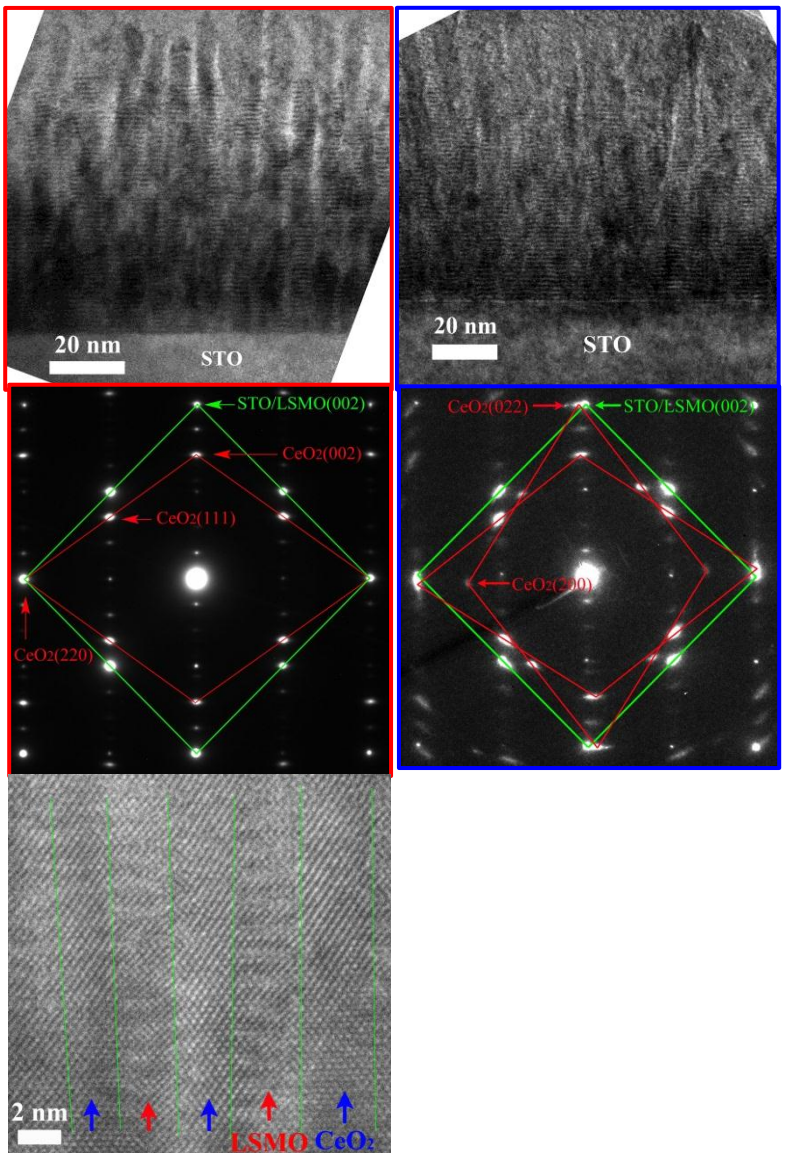

FIG. 2. (a) and (b) TEM images for the VAN films deposited at 1 Hz and 10 Hz, respectively. (c) and (d) SAED patterns of the 1 Hz and 10 Hz samples, respectively. (e) High resolution TEM image show the high quality heteroepitaxial growth of VAN film.

Temperature dependence of resistivity (ρ-T) for VAN film deposited at different laser frequencies shown in the inset of Fig. 3(b). It shall be noted that the metal-insulator transition temperature shifts to lower temperature as the laser repetition rate increases, indicating the reduced domain size and the increase of phase boundary effect.[9] Fig. 3(b) shows the ρ-T curves of 10 Hz VAN films and the temperature dependence of magnetoresistance (MR-T). The MR of 10 Hz VAN films (~21 % at 20 K), conformed by field-dependent measurements [Fig. 3(c)], is far larger than that of PE LSMO. The curve in Fig. 3(c) presents the well-defined magnetic hysteresis loop of the 10 Hz VAN films at 20 K. It is noted that the MR is proportional to the $(M/M_S)^2$, where M_S is the saturation magnetization. It is clear that the MR (20 K) of all VAN films are larger than that of PE LSMO films [Fig. 3(d)]. The MR increases as the deposition frequency increases can be attributed to the increased doupling of LSMO nanodomains due to the reduced domain size and enhanced disorder in phase boundary regions.

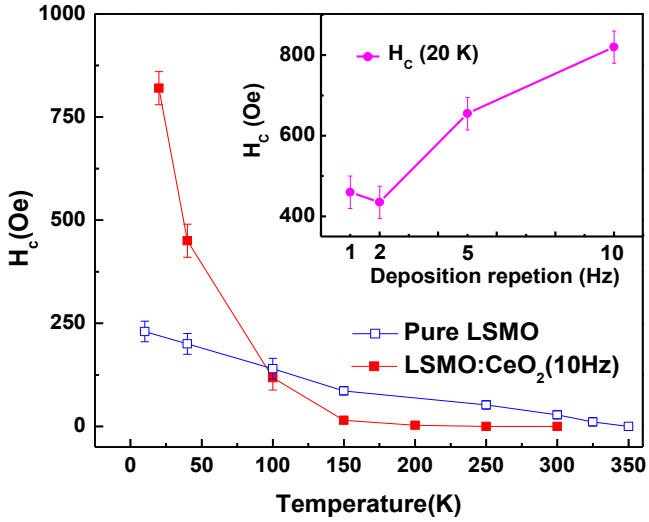

FIG. 3. (a) H_C-T for PE LSMO film and 10 Hz LSMO:CeO_2 VAN film. Inset of (a): deposition frequency dependence of H_C for VAN films. (b) ρ-T and MR-T curves for 10 Hz deposited VAN film. MR=$(\rho_0-\rho_H)/\rho_0$, where ρ_0 and ρ_H are the resistivity in a zero field and in a finite field, respectively. (c) Field dependence of MR measurement at 20 K for 10 Hz LSMO:CeO_2 VAN film and PE LSMO film. This isothermal MR curve shows a butterfly profile. The blue line represents magnetic hysteresis loop for this sample measured at the same temperature. (d) Relationship between MR (20 K) and deposition repetition. The dash line is the reference MR (20 K) value for PE LSMO film on STO substrates.

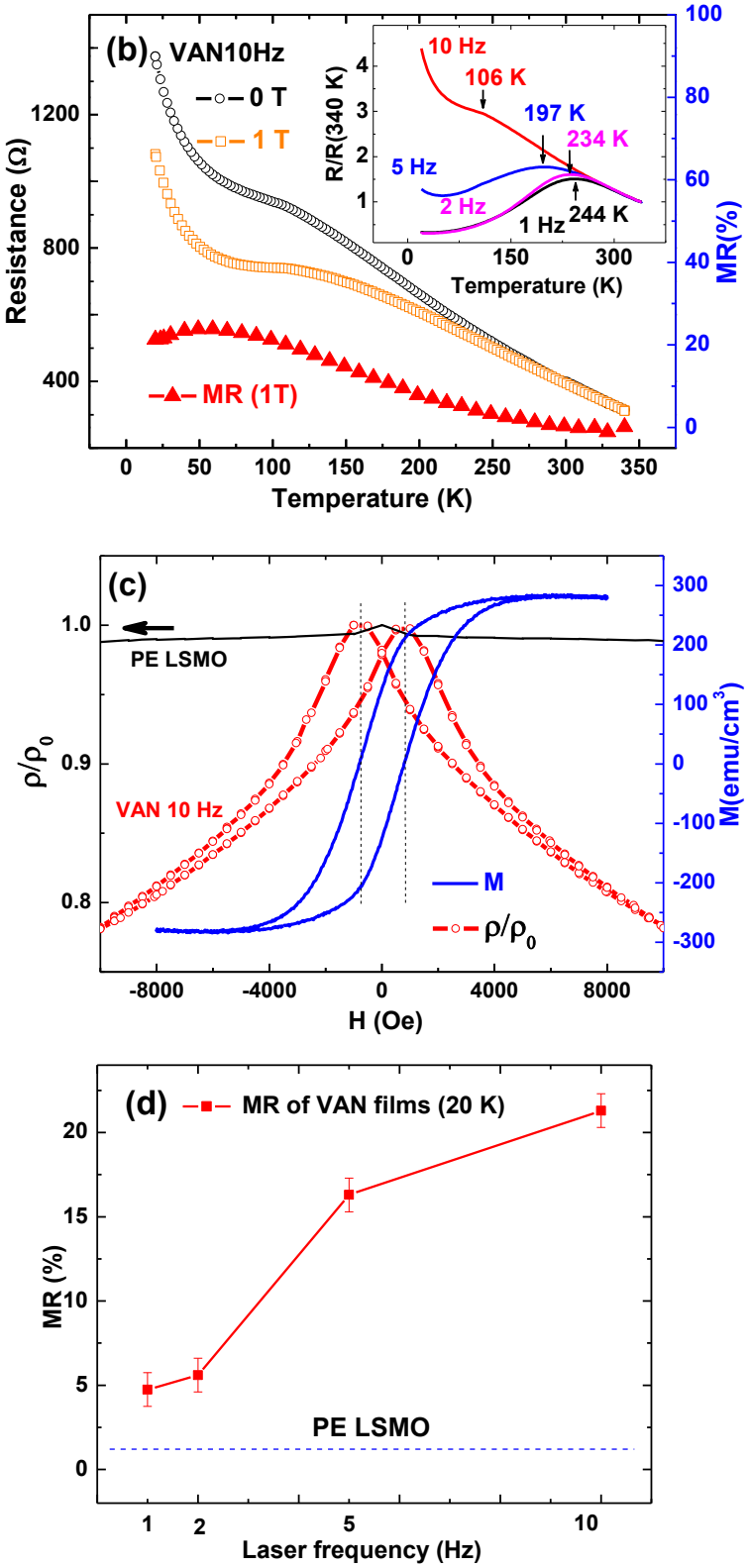

FIG. 3. Continued.

CHAPTER IV

SUMMARY AND CONCLUSIONS

It has been widely reported that the low field magnetoresistance (LFMR) effect exists in the bulk perovskite manganites or their polycrystalline and nanocrystalline films. [10] It is also well known that LFMR in PE LSMO is negligible due to the absence of high angle grain boundary (HAGB). And even in some LCMO nanocomposite films, there was no obvious LFMR observed due to the missing of HAGB in the epitaxial composite films. [11] In our case, the large LFMR at low temperature in epitaxial LSMO:CeO_2 VAN films might have a different mechanism, different from the MR in their polycrystalline counterparts which stems from the HAGB. [10] In the VAN structure, the epitaxial ferromagnetic nanodomains are separated by CeO_2 insulating phases, and thus, long range double exchange interaction is supressed due to the termination of LSMO crystal structure, the broken Mn-O-Mn spin chains, and the exist of spin/structural disorders at the phase boundaries region. The relative angle between magnetic momentums of neighboring nanodomains is not zero since the decoupled ferromagnetic nanodomains have different shape, size, and local strain. In other words, PE LSMO films exhibit a single magnetic domain due to the strong dipolar coupling while LSMO phase in epitaxial VAN system show multidomains with unparallel magnetic momentums, which were vertically network sandwiched by CeO_2 insulating phases. Thus, it is reasonable to argue that spin dependent tunneling across the insulating CeO_2 phase is responsible for the LFMR effect which is similar with the tunneling-type giant MR in granular systems or ferromagnetic tunnel junctions. [12]

In conclusion, herteroepitaxial LSMO:CeO_2 films with self-assembled VAN structure were grown on STO (001) substrates by PLD. The enhanced coercivity and LFMR are largely due to the strong interaction between the pervoskite and the secondary phase. The results suggest that two-phase VAN structure provides a promising way to explore new functionality which may not obtain in the single-phase epitaxial thin films.

REFERENCES

[1] a) H. Zheng, F. Straub, Q. Zhan, P. Yang, W. Hsieh, F. Zavaliche, Y. Chu, U. Dahmen, and R. Ramesh, Adv. Mater. **18**, 2747 (2006). b) H. Zheng, Q. Zhan, F. Zavaliche, M. Sherburne, F. Straub, M.O. Cruz, L.Q. Chen, U. Dahmen, R. Ramesh, Nano Lett. **6**,1401 (2006). c) I. Levin, J. H. Li, J. Slutsker, and A. L. Roytburd, Adv. Mater. **18**, 2044 (2006). d) L. Yan, F. M. Bai, J. F. Li, and D. Viehland, J. Am. Ceram. Soc. **92**, 17 (2009).

[2] a) Q. Zhan, R. Yu, S. P. Crane, H. Zheng, C. Kisielowski and R. Ramesh, Appl. Phys. Lett. **89**, 172902 (2006). b) L. Mohaddes-Ardabili, H. Zheng, S. B. Ogale, B. Hannoyer, W. Tian, J. Wang, S. E. Lofland, S. R. Shinde, T. Zhao, Y. Jia, L. Salamanca-Riba, D. G. Schlom, M. Wuttig and R. Ramesh, Nature Mater. **3**, 533 (2004). c) L. Yan, Y. D. Yang, Z. G. Wang, Z. P. Xing, J. F. Li and D. Viehland, J. Mater. Sci. **44**, 5080 (2009).

[3] H. Zheng, J. Wang, S. E. Lofland, Z. Ma, L. Mohaddes-Ardabili, T. Zhao, L. Salamanca-Riba, S. R. Shinde, S. B. Ogale, F. Bai, D. Viehland, Y. Jia, D. G. Schlom, M. Wuttig, A. Roytburd and R. Ramesh, Science **303**, 661 (2004).

[4] Q. Zhan, R. Yu, S. P. Crane, H. Zheng, C. Kisielowski and R. Ramesh, Appl. Phys. Lett. **89**, 172902 (2006).

[5] a) H. Yang, H. Y. Wang, J. S. Yoon, Y. Q. Wang, M. K. Jain, D. M. Feldmann, P. C. Dowden, J. L. MacManus-Driscoll and Q. X. Jia, Adv. Mater. **21**, 3794 (2009). b) J. L. MacManus-Driscoll, P. Zerrer, H. Y. Wang, H. Yang, J. Yoon, A. Fouchet, R. Yu, M. G. Blamire and Q. Jia, Nature Mater. **7**, 314 (2008).

[6] a) H. Kim, L. Bi, H. Paik, D. Yang, Y.C. Park, G. F. Dionne and C. A. Ross, Nano Lett. **10**, 597, (2010). b) L. Bi, H. Kim, G. F. Dionne, C. A. Ross, H. Paik and Y.C. Park, Appl. Phys. Lett. **95**, 121908 (2009).

[7] a) Y. S. Du, B. Wang, T. Li, D. B. Yu, and H. Yan, J. Magn. Magn.Mater. **297**, 88 (2006). b) R. Moubah, S. Colis, C. Ulhaq-Bouillet, M. Drillon, and A. Dinia. J. Phys. Chem. C. **114**, 1684 (2010).

[8] L. M. Berndt, Vincent Balbarin, and Y. Suzuki, Appl. Phys. Lett. **77**, 2903 (2000).

[9] a) H. Yang, Z. E. Cao, X. Shen, T. Xian, W. J. Feng, J. L. Jiang, Y. C. Feng, Z. Q. Wei, and J. F. Dai, J. Appl. Phys. **106**, 104317 (2009). b) J. Y. Gu, C. Kwon, M. C. Robson, Z. Trajanovic, K. Ghosh, R. P. Sharma, R. Shreekala, M. Rajeswari, T. Venkatesan, R. Ramesh, and T. W. Noh, Appl. Phys. Lett. **70**, 1763 (1997).

[10] a) LI. Balcells, A. E. Carrillo, B. Martínez, J. Fontcuberta, Appl. Phys. Lett. **74**, 4014 (1999). b) L. D. Yao, W. Zhang, J. S. Zhang, H. Yang, F. Y. Li, Z. X. Liu, C. Q. Jin, and R. C. Yu, J. Appl. Phys. **101**, 063905 (2007).

[11] V. Moshnyaga, B. Damaschke, O. Shapoval, A. Belenchuk, J. Faupel, O. I. Lebedev, J. Verbeeck, G. van Tendeloo, M. Mücksch, V. Tsurkan, R. Tidecks, and K. Samwer, Nature Mater. **2**, 247 (2003).

[12] H. Fujimori, S. Mitani, and S. Ohnuma, Mater. Sci. Eng., B **31**, 219 (1995).

CONTACT INFORMATION

Name:	Harshad Hazariwala
Professional Address:	c/o Dr. Haiyan Wang Department of Electrical and Computer Engineering Texas A&M University College Station, TX 77843-3128 Office: 979-845-5082 Fax: 979-845-6259
Email Address:	wangh@ece.tamu.edu
Education:	B.A., Electrical Engineering, Texas A&M University, May 2011 Undergraduate Research Scholar